Simulation of snow and soil water content as a basis for satellite retrievals

M. J. Sandells, G. N. Flerchinger, R. J. Gurney and D. Marks

ABSTRACT

It is not yet possible to determine whether global snow mass has changed over time despite collection of passive microwave data for more than thirty years. Physically-based, but computationally fast snow and soil models have been coupled to form the basis of a data assimilation system for retrievals of snow mass and soil moisture from existing and future satellite observations. The model has been evaluated against observations of snow mass and soil temperature and moisture profiles from Reynolds Creek Experimental Watershed, Idaho. Simulation of snow mass was improved early in the season due to more realistic representation of soil heat flux, but led to an overestimation of snow mass later in the season. Soil temperatures were generally simulated well; freezing of the surface layers was not observed but was simulated, which affected soil water transport. Limited knowledge of the soil lower boundary conditions is acceptable for snow mass and surface soil moisture retrievals, although improvements are required for more accurate simulations of deeper soil moisture at this site. Development of a data assimilation framework to retrieve snow mass and near-surface soil moisture is discussed.

Key words | boundary conditions, physically-based model, remote sensing, snow, soil moisture

M. J. Sandells (corresponding author)
R. J. Gurney
National Centre for Earth Observation,
Environment Systems Science Centre,
Harry Pitt Building,
Whiteknights,
PO Box 238,
Reading,
RG6 6AL, UK
E-mail: *m.j.sandells@reading.ac.uk*

G. N. Flerchinger
D. Marks
USDA-ARS Northwest Watershed Research Center,
800 Park Boulevard,
Suite 105,
Boise,
Idaho 83712,
USA

INTRODUCTION

Snowmelt is a vital resource, with over one sixth of the world's population dependent on melt from snow and glaciers for their water source (Barnett *et al.* 2005). With a warming climate, changes are expected to occur in the rates of snow accumulation and melt resulting in alterations to the current annual groundwater recharge regime. Nayak *et al.* (2010) analysed forty-five years of precipitation, temperature and streamflow data from a northwestern US mountain catchment to show that whilst the magnitude of precipitation had not changed significantly, the proportion of precipitation that was snow had decreased at all elevations in the watershed. Whether as soil moisture or snow, monitoring of the water stored in the land surface is crucial to optimise its use.

Passive microwave satellite observations of the land surface have been made over a range of frequencies since 1978 with the launch of scanning multichannel microwave radiometer (SMMR). These and subsequent observations have been used to retrieve snow mass. In 2009, the soil moisture ocean salinity (SMOS) mission was launched, and measures the microwave brightness temperature at 1.4 GHz. The accuracy of the SMOS instrument is still under assessment, but Davenport *et al.* (2010) have investigated the accuracy of snow mass retrievals based on earlier work by Chang *et al.* (1987) and found that snow mass was overestimated by a factor of 2–3. An alternative approach for retrievals of snow and soil moisture is to use data assimilation techniques, where a physically-based model of the land surface can be used to give an estimate of parameters with greatest sensitivity, for example the size of the snow grains. These parameters can then be used to drive a microwave emission model in order to retrieve the water content of the land surface from the satellite observations.

This paper describes the physical basis of the underlying model that will be used in the data assimilation framework

doi: 10.2166/nh.2012.028

currently under development. A computationally efficient model of the snow was chosen for this purpose, but as it does not represent the soil explicitly and requires observations of near-surface soil temperatures (which are generally not available) to drive the model, it was coupled with a physically-based model of the soil. Soil temperature can have a critical influence on the establishment of the snowpack early in the season, and can lead to biases in the snow mass throughout the season, as is shown in this paper. Unfortunately the effect of soil heat flux on the development of the snowpack has been rather overlooked to date, although many studies have looked at the effect of snow on the soil (e.g. Zhang 2005). Male (1980) indicated that the soil heat flux, whilst small, can have a significant effect cumulatively over a season. Despite this, the soil heat flux has been treated as a constant in some models (Brun *et al.* 1989) or neglected (Liang *et al.* 1994).

An evaluation of the coupled and uncoupled model against field observations of snow mass and soil temperature and moisture profiles is presented in this paper. One key question in the use of models in data assimilation is how well the model performs when very little prior information is known about the land surface. Here, the hypothesis is that given a deep enough lower boundary in the soil, the boundary conditions do not affect the soil temperature and moisture at the surface and near-surface. This hypothesis has been tested and errors in the simulations from uncertainties in the soil lower boundary condition are presented. Finally, formation of the data assimilation framework is discussed.

METHODS

To form the Snow-SVAT (Snow-Soil-Vegetation-Atmosphere Transfer) scheme to be used in the data assimilation system, a physically-based, but computationally simple, snow model was chosen and coupled with a physically-based multi-layer soil model. In this section, the physics behind the snow and soil models is presented, and the mechanism of coupling between the models is discussed. Field data used to test the model and field site characteristics are described. This paper addresses the question of how well the lower boundary conditions need to be known, so the approach of this study is also outlined in this section.

Snow model: SNOBAL

The dual-layer snow model chosen to form the data assimilation system is SNOBAL (Marks & Dozier 1992; Marks *et al.* 1998). The snowpack is represented by two layers: a thin surface layer where the surface energy exchanges occur, and a thicker base layer that contains the bulk of the snow. Energy balance for the snowpack is given by Equation (1), where ΔQ is the change in snowpack energy (this results in a change in temperature if the snow is below freezing, or a change in phase if the snow is at the freezing point), S_{net} is the net radiative flux (solar and thermal), H and L_vE are the sensible and latent heat transfers, G is the soil heat flux and M is the heat advected by precipitation.

$$\Delta Q = S_{net} + H + L_vE + G + M \quad (1)$$

Forcing data are derived from meteorological measurements of downwelling solar radiation ($R\downarrow$), thermal radiation, wind speed, air temperature and humidity. At present, reflected solar radiation ($R\uparrow$) is calculated prior to the simulation from Equation (2), where α is the albedo. Separate albedos are calculated for the visible and near-infrared frequencies (Equations (3) and (4)), and 48% of the incoming solar radiation is assumed to be in the visible part of the spectrum, which is consistent with field observations at a ridge site between November and May by Marks & Dozier (1992; Table 1).

$$R\uparrow = \alpha R\downarrow \quad (2)$$

Table 1 | Root Mean Squared Differences between simulated and observed snow mass from the snow pillow for periods where snow was observed, and from establishment of snowpack to peak SWE. Different SHAW limits represent dewpoint temperature thresholds above which precipitation is assumed to be rain.

Model	RMSD (mm) (snow period)	RMSD (mm) (to peak SWE)
SNOBAL	30	17
SNOBAL-SHAW	49	44
SHAW (0 °C limit)	74	19
SHAW (0.5 °C limit)	74	40

$$\alpha_{\text{vis}} = \alpha_{\text{vis}}^{\max} - 0.002r^{1/2} \quad (3)$$

$$\alpha_{\text{nir}} = \alpha_{\text{nir}}^{\max} \times \exp[-02123r^{1/2}] \quad (4)$$

Maximum albedos for visible ($\alpha_{\text{vis}}^{\max}$) and near-infrared ($\alpha_{\text{nir}}^{\max}$) are assumed to be 1.0 and 0.85447, respectively. r is the effective grain radius, which is subject to growth between precipitation events. Snow ageing, or the change in radius, is calculated from functions derived from Dozier *et al.* (1981) with grain growth effects on broad-band reflectance reported in Marshall & Warren (1987).

Turbulent transfer of sensible and latent heat is estimated from measurements of wind speed, temperature and vapour pressure at a single height, through calculation of the Obukhov stability length, as described by Marks & Dozier (1992). This method was chosen because it proved to be the most numerically stable, particularly for high wind speed conditions over snow. A roughness value of 3 mm was chosen for the smooth snow surface for the simulations presented in this paper, as this parameter has been used in other simulations and we have chosen not to calibrate the model further. The impact of the uncertainty in turbulent transfer parameters on the energy balance is small over snow as the sensible and latent heats are generally opposite in sign (Marks & Dozier 1992). Soil heat flux is determined from discretisation of the heat conduction equation, which results in Equation (5), where k is the thermal conductivity, T is the temperature, Δz is the thickness of the layer, and subscripts s and g represent the snow and soil (ground), respectively.

$$G = \frac{2k_s k_g (T_g - T_s)}{k_s \Delta z_g + k_g \Delta z_s} \quad (5)$$

Measured precipitation data are also used as forcing data. The proportion of snow and rain, and density of the freshly fallen snow is determined from the dewpoint temperature, according to the relationships given in Table I of Marks *et al.* (1999). Densification of the snow cover is simulated, using the density-time curve given in Equation (6), where ρ_s is the snow density, t is time in seconds, $\rho_{s,\max}^{\text{grav}}$ is the maximum density due to compaction by gravity (assumed to be 350 kg m^{-3}) and τ is a constant that represents the time taken for half the maximum density to be reached (assumed to be 10 days). Addition of fresh, lower density snow is accounted for by recalculating the position along the time-density curve.

$$\rho_s(t) = \frac{\rho_{s,\max}^{\text{grav}}}{1 + \tau/t} \quad (6)$$

Under melt conditions, liquid water contributes to the densification process, and this is simulated according to Equation (7), where $\rho_{s,\max}^{\text{melt}}$ is the maximum density from melt processes (assumed to be 550 kg m^{-3}), β is an empirically-derived parameter that controls the rate of densification (assumed to be 0.4), and B is the ratio of the mass of liquid water added to the snow from melt and rain to the mass of the snowcover.

$$\Delta\rho_s = \frac{\rho_{s,\max}^{\text{melt}} - \rho_s}{1 + \beta/\text{B}} \quad (7)$$

SNOBAL is computationally efficient, has been tested extensively and has been used to simulate the areal depletion of snow in a semi-arid mountain basin (Winstral & Marks 2002), so is suitable for incorporation in the data assimilation system.

Soil model: SHAW

In order to provide soil temperatures for calculation of the soil heat flux and to form the basis of a soil moisture retrieval system, a multilayer soil model was chosen to couple with SNOBAL. The model selected is the Soil Heat and Water model (SHAW). SHAW (Flerchinger & Saxton 1989) was designed specifically to simulate the freezing and thawing of the soil and has a physical basis, so is a good candidate for coupling with SNOBAL. Although SHAW contains a vegetation component, a snow component and is capable of simulating the transport of solutes, these components are deemed to be surplus to requirements for inclusion in the data assimilation system and have not been implemented in this application. SNOBAL was used in lieu of the multilayer snow model of SHAW because of its computational efficiency. Similar to the snow model, SHAW is based on

conservation equations for mass and energy. An implicit finite-difference scheme is used to discretise the conservation equations, which are then solved iteratively with a Newton–Raphson approach, as described in Flerchinger (2000). The energy balance at the soil surface is driven by meteorological measurements of incoming solar radiation, wind speed, air temperature, humidity and precipitation. Although downwelling thermal radiation is simulated in SHAW, for this adaptation measurements are used as forcing data to be consistent with the SNOBAL driving data. Additionally, the rain/snow threshold temperature in SHAW has been adapted for comparisons in this paper. Here, dewpoint temperature rather than the physical temperature is used, and threshold limits of 0° C and 0.5 °C have been considered. These are not directly comparable with SNOBAL, which assumes mixed rain/snow precipitation for dewpoint temperatures between −0.5 and 0.5 °C, but is a good approximation.

Soil water mass conservation is given by Equation (8), where the terms are the net liquid flux, net vapour flux, source/sink (U) term, change in liquid content and change in ice content. K is the hydraulic conductivity, z is the soil depth, ρ_l and ρ_i are the densities of water and ice, q_v is the vapour density of air voids, θ_l and θ_I are the volumetric fractions of liquid and ice, and t is time. The matric water potential, Ψ, is calculated from the liquid water content, from Equation (9), where the air entry potential (Ψ_e) and the pore-size distribution index (b) are required as input parameters, and the saturated water content (θ_s) is defined from the bulk density of the soil (another input parameter).

$$\frac{\partial}{\partial z}\left[K\left(\frac{\partial \Psi}{\partial z}\right)+1\right]+\frac{1}{\rho_l}\frac{\partial q_v}{\partial z}+U=\frac{\partial \theta_l}{\partial t}+\frac{\rho_i}{\rho_l}\frac{\partial \theta_i}{\partial t} \quad (8)$$

$$\Psi=\Psi_e\left(\frac{\theta_l}{\theta_s}\right)^{-b} \quad (9)$$

Infiltration of liquid water into the soil is calculated using the Green-Ampt equation (under the assumption of zero matric potential at the wetting front), and redistribution of infiltrated water is accomplished through discretisation of the Richardson equation. A full description of the model is given in Flerchinger (2000).

Coupling between SNOBAL and SHAW

SNOBAL and SHAW are linked through the energy and mass balances. Soil temperature calculated by SHAW is used to determine the soil heat flux (Equation (5)), which affects both snow and soil temperatures. Outflow from the snowpack is used to provide the upper boundary condition for the solution of the SHAW mass balance. Although SHAW calculates the temperature of the soil surface, the temperature at a depth of 30 cm is used to determine the soil heat flux. This is not ideal, as it smears the temperature gradient across the snow – soil interface, but a necessary compromise as the structure of the two models are not completely compatible. This is discussed later in the paper. For calculation of soil heat flux, soil thermal conductivity (k_g) in SNOBAL is represented by a constant value (k_c) with an empirical correction for vapour diffusion effects (D_e is an effective diffusion coefficient), as given by Equation (10).

$$k_g = k_c + L_v D_e q_v \quad (10)$$

The default value of k_c in SNOBAL was reduced from the moist sand value of 1.65 J m^{-1}s^{-1}k^{-1} to the dry sand value of 0.3 J m^{-1}s^{-1}K^{-1} so that k_g was similar in magnitude to the SHAW soil thermal conductivity (which is derived from the DeVries method).

Hourly meteorological data are used to drive the model, although the computational timestep is subdivided as is needed for computational stability for thin layers. The subdivided timesteps and mass thresholds can be specified, but here the default values were used, where the timestep decreases from hourly to 15 minutes when the mass of a layer is <60 kg m^{-2}, and to 1 minute timesteps when a layer mass is <10 kg m^{-2}. The two models have been loosely coupled, where the soil mass and energy balances are determined at the end of the timestep for the snow model, i.e. the snow properties are updated for the change over the hour first, then soil properties are updated. Although this means that the soil temperature used to compute the soil heat flux may be lagged by up to an hour, the mean magnitude of difference in measured temperature at a depth of 30 cm in the soil is 0.01 K. Whilst rigorous coupling of the

models, where the mass and energy balances of the snow and soil are solved simultaneously is more physically realistic, the increase in computational expense required to do this is not justified for the application for which the model is designed.

Evaluation of coupled model and lower boundary conditions

The coupled model has been evaluated against measurements of snow water equivalent (SWE), soil heat flux, and profiles of soil temperature and moisture at a point. The site chosen was the Reynolds Mountain East catchment in Idaho, USA, from 1st October 2005 to 30th June 2006. This site was chosen because of the high quality of data and the availability of concurrent snow and soil data at the same location. SWE was measured with a snow pillow. Although difficult to quantify a precise error due to differences in sample location and sampling techniques, the uncertainty associated with the snow pillow measurements is estimated to be approximately ±5%. Additional errors are incurred for shallow snow (SWE <100 mm), where solar penetration through the snow and the vapour barrier at the snow base result in diurnal melt – freeze cycles and poor physical contact between the snow and instrument. The pressure transducer is also sensitive to temperature fluctuations in shallow snow. As the snowpack increases in mass, these effects are minimised.

Soil heat flux was measured with two Hukseflux heat flux plates installed 6 cm deep within the soil. Soil temperature and moisture were measured at 3, 15, 30, 52, 78 and 97 cm with Hydraprobes. The accuracy of the temperature measurements is dependent on the temperature, but is ±0.2 °C around 0 °C. The uncertainty in the soil moisture measurements, which have been determined from the dielectric constant measurements with Equation (11) (from Seyfried *et al.* 2005), has been found to be 0.02 m^3/m^3, where θ is the volumetric soil water content and ε_r' is the real part of the dielectric constant.

$$\theta = 0.109\sqrt{\varepsilon_r'} - 0.179 \quad (11)$$

These measurements at different depths in the soil were used to define soil nodes at 0 cm, 3 cm, 9 cm, 15 cm, 30 cm, 50 cm, 80 cm and 1 m. Measurements of the temperature and moisture at 97 cm form the lower boundary conditions for the model, and are shown in Figure 1 (T_meas for the temperature in Figure 1(a) and SM_meas for the moisture in Figure 1(b)). These sensors are all located at a point that has a low elevation in the basin. Bathurst & Cooley (1996) hypothesised different representations of the sub-surface flow and soil permeability in this basin and found that rapid sub-surface drainage channels best explained the observed hydrographs. This hypothesis is consistent with a large increase in observed soil moisture at the lower boundary in this dataset, as shown by Figure 1(b).

For global retrievals of snow mass and soil moisture, soil parameters and lower boundary conditions are unlikely to be known. In this paper, we address the question of how well the lower boundary temperature and moisture need to

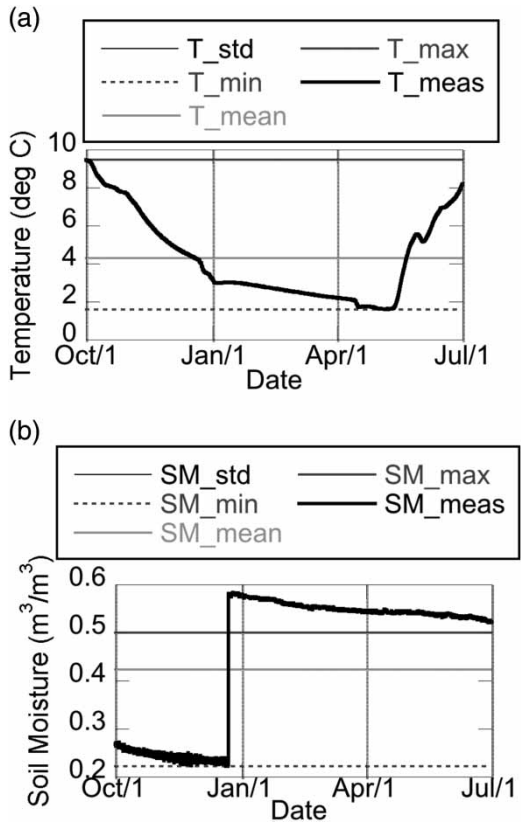

Figure 1 | Soil lower boundary conditions for (a) temperature (T) and (b) soil moisture (SM). Standard (std) conditions were used to evaluate the model and equal the measurements (so are overlain in this plot), except SM was limited to a maximum of 0.5 m^3/m^3 (and is overlain by SM_max). Min, mean and max conditions were used to test the model sensitivity to the lower boundary conditions.

be known by assuming that either the mean is known (analogous to climatology inputs), or the minimum or maximum (analogous to a single point measurement). Figure 1 shows the lower boundary scenario for all simulations, including the standard model runs where the boundary conditions are known. As the maximum measured soil moisture is higher than is physically possible for the model parameters (the measured moisture is larger than the pore space in the soil), the lower boundary soil moisture is limited to 0.5 m^3/m^3, which is used as the upper limit of permissible soil moisture in the SMOS mission. Results from the simulations are presented in the following section.

RESULTS

Model evaluation

Evaluation of the coupled model against SWE is shown in Figure 2. SWE is the depth of water that would result if the snow melted, and is synonymous with snow mass. Figure 2 illustrates the simulation of SWE for the uncoupled SNOBAL, the stand alone SHAW and for the coupled SNOBAL-SHAW simulations. Root mean squared differences (RMSD) are given in Table 1 for the period where the snowpack was present according to the observations (3rd November 2005–16th May 2006), and for the period from snowpack establishment to peak SWE (3rd November 2005–12th April 2006). RMSD are reduced if the melt period is excluded, although the difference is small for the SNOBAL-SHAW simulations. The two precipitation thresholds chosen for SHAW, as shown in Figure 2, have a large effect on the SWE. For the lower, 0 °C limit, more precipitation is assumed to be rain. This reduces the bias in the SWE and for the accumulation period, SHAW shows good agreement with the snow pillow observations (similarly to SNOBAL). At the higher threshold limit, more precipitation is assumed to be snow. This increases the overall SWE in the accumulation period and the RMSD for this SHAW simulation is similar to the RMSD for the SNOBAL-SHAW simulation.

Compared to the continuous measurements from the snow pillow, the RMSD for the SNOBAL simulation was 30 mm for the period where the snowpack was established in the observations. For the coupled SNOBAL-SHAW simulation, the RMSD was higher (49 mm) due to an overestimation in SWE from the middle of December until the middle of the ablation period. This is in contrast to the SNOBAL simulation, where snow mass was underestimated early in the season until the middle of December. Figure 3 shows simulation of SWE more clearly for the initial snowpack formation.

Three melt periods have been identified in Figure 3, where the rate of observed snow melt has not been captured adequately by the model. Early in the season, diurnal fluctuations occurred in the observed snow mass, which are a result of shallow snow problems (as discussed in the methods section). In late November (period A), the observations do not show significant melt. SWE simulated by SNOBAL was reduced from 52.2 mm (13th November) to 24.5 mm (25th November). Melt losses simulated by the coupled model in this period were less, and SWE was reduced from 69.5 to 61.2 mm. Observations indicate that melt occurred in early December (period B), although this was not simulated by SNOBAL nor the coupled SNOBAL-SHAW model. In late December (period C) melt was observed and simulated, although the rate of melt was underestimated by similar amounts in both models. The differences between simulated and observed SWE at the end of period C generally set the biases in the two models until around maximum SWE. Differences between the SNOBAL and SNOBAL-SHAW simulations arise from the soil heat flux, which primarily result from changes in the soil thermal conductivity and the soil temperature.

Soil heat flux simulated by SNOBAL, SNOBAL-SHAW and SHAW is shown in Figure 4 and compared to the mean of the measurements from the two heat flux plates. For SHAW, the 0.5 °C rain/snow precipitation threshold simulation was chosen as it was most similar to the SNOBAL-SHAW simulations. Although the heat flux plates were at a soil depth of 6 cm, the simulated soil heat flux from SHAW was comparable to the observations. Soil heat flux simulated by SNOBAL-SHAW was slightly greater in magnitude and more variable than that simulated by SHAW. The heat flux simulated by SNOBAL was larger than that simulated by SNOBAL-SHAW. As the snowpack became deeper, the soil heat flux was reduced to a near-negligible value, although this occurred later in the SNOBAL and

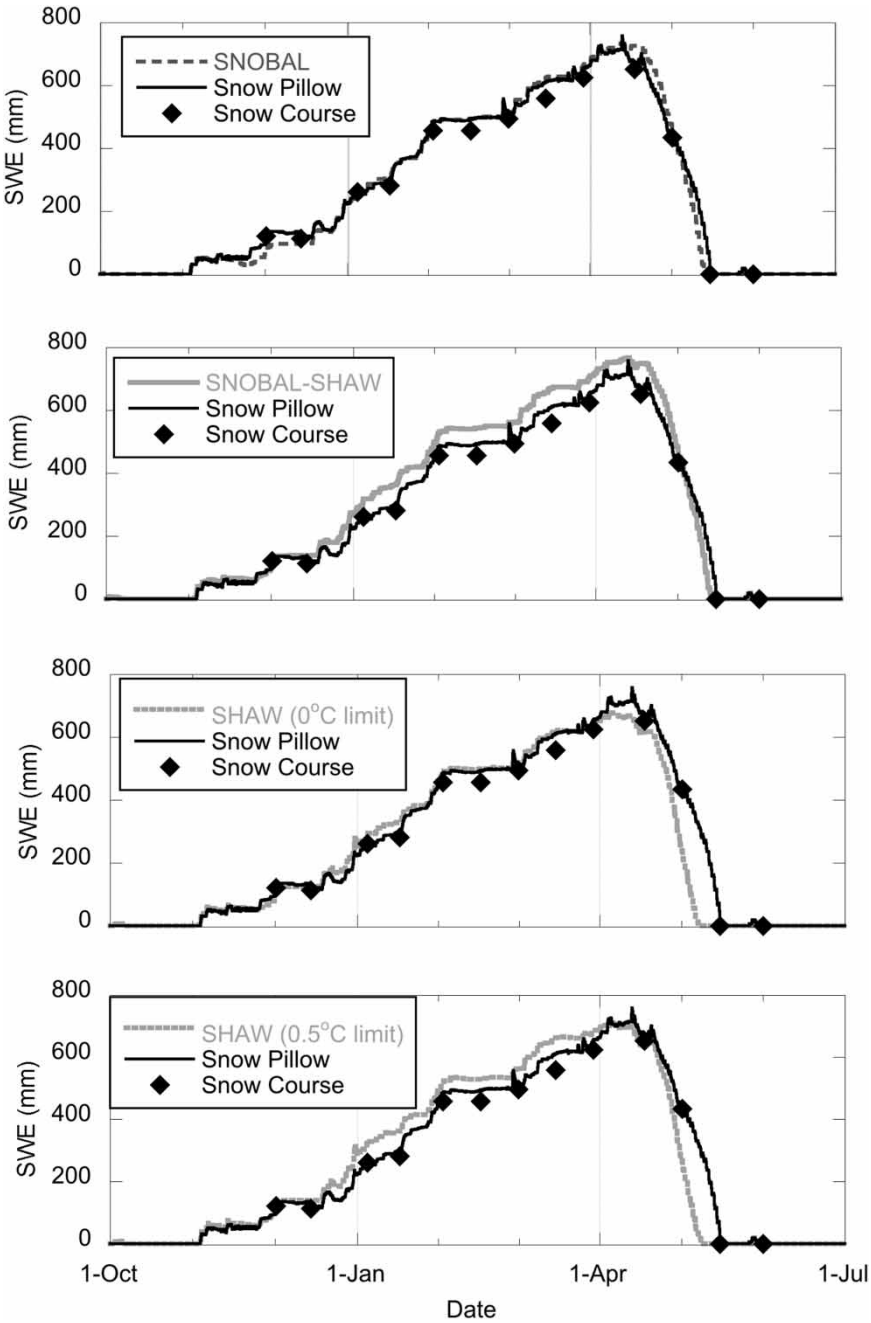

Figure 2 | Comparison between simulated and observed snow mass for SNOBAL, SHAW and the coupled SNOBAL-SHAW model. SHAW has been adjusted to ingest similar forcing data to SNOBAL and SNOBAL-SHAW, although two different dewpoint temperature limits of 0 and 0.5 °C have been chosen to differentiate between snow and rain precipitation events.

SNOBAL-SHAW simulations of the snow – soil interface than in the observations at a depth of 6 cm.

Figure 5 illustrates the change in soil moisture and temperature at different depths in comparison to Hydraprobe observations. Initialisation of the snowpack occurs at the point where the soil surface temperature drops to zero. Although the diurnal dynamic range of surface temperature (3 cm) and near-surface temperature (15 cm) is larger than observed during snow-free periods, warming and cooling trends in the simulations are consistent with the

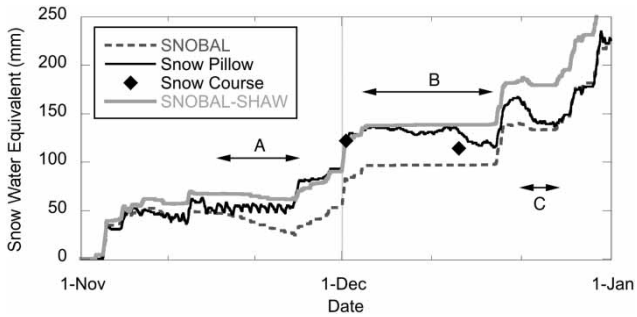

Figure 3 | Simulation of snow water equivalent during establishment of snowpack. Three periods (A, B, C) are shown where rate of snow melt is not represented accurately.

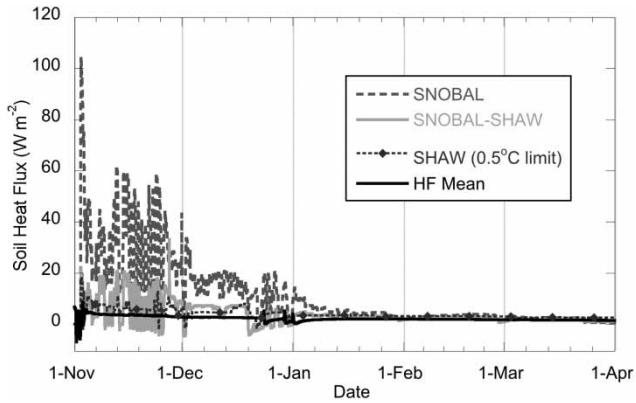

Figure 4 | Comparison between the mean of two sets of measurements from Hukseflux heat flux plates (HF Mean) and simulations of soil heat flux from SNOBAL, SNOBAL-SHAW and SHAW (where precipitation is assumed to be rain if the dewpoint temperature is above 0.5 °C). Positive heat flux represents energy transfer into the snow.

observations. Deeper in the soil, there is also a warm bias in the snow-free periods, and observed cooling dips in the observations at the end of the season are also simulated at all depths. For the period with an established snowpack, simulated soil temperatures were generally in good agreement with the observations at all depths. RMSD for the snow-free and established snowpack periods are given in Table 2 and range from 0.8 to 5.3 °C (snow-free) and 0.3 to 1.3 °C (snow present), with the larger errors in the soil surface layers. However, some freezing of the soil was simulated to a depth of 9 cm but was not observed, suggesting that Equation (5) overestimated heat flux from the soil to the snowpack. Consequently, this has an impact on soil moisture, which is also shown in Figure 5.

Wetting of the surface is simulated and observed in the last week of October and the first week in November. Infiltration into the near-surface soil at 15 cm is simulated in the second to third week of November, which is consistent with the observations. However, the observed wetting of the soil surface on the 25th November was not simulated. This occurred as a result of simulated freezing in the surface and near-surface soil. Figure 6 indicates the increase in ice content for the 3 cm soil depth, along with the additional 0 and 9 cm soil nodes used in the model but not validated because observations were not made at these soil depths. Soil freezing was not simulated at a soil depth of 15 cm. Conversion of liquid soil moisture to ice at the 3 cm depth prevented infiltration to the 15 cm depth in the simulations. Therefore, the observed increase in soil moisture at 15 cm on the 25th November was not captured by the simulations.

As the soil surface thawed from the 19th December onwards in the simulations, moisture was released from the ice, shown by increasing 3 cm soil moisture in Figure 5. However, by this stage the lower soil layers were saturated in the simulations, so the surface moisture did not infiltrate and drain to the lower layers. As a result, the simulated 3 cm soil moisture was higher than the observed values.

Saturation of deep soil in late December occurred in the observations. Figure 7 shows initial saturation at a depth of 1 m early on the 22nd December. The wetting front then propagated upwards through the soil over the course of the day. Snow meltwater infiltrated the soil on the 21st December, to a depth of 15 cm on the 22nd. This observed behaviour was also captured by the model, as shown in Figure 5, although propagation of the wetting front was slower in the simulation. Saturated soil moisture was simulated well at depths of 15 and 30 cm, but the model cannot simulate the extreme soil moistures observed at 50 cm, 80 cm and 1 m due to insufficient void space in the simulated soil matrix.

Model sensitivity to lower boundary conditions

The previous section demonstrated how well the SNOBAL-SHAW coupled model is able to simulate SWE and profiles of soil temperature and moisture, given well specified lower boundary conditions, and also highlighted limitations of the model. This simulation is henceforth referred to as the

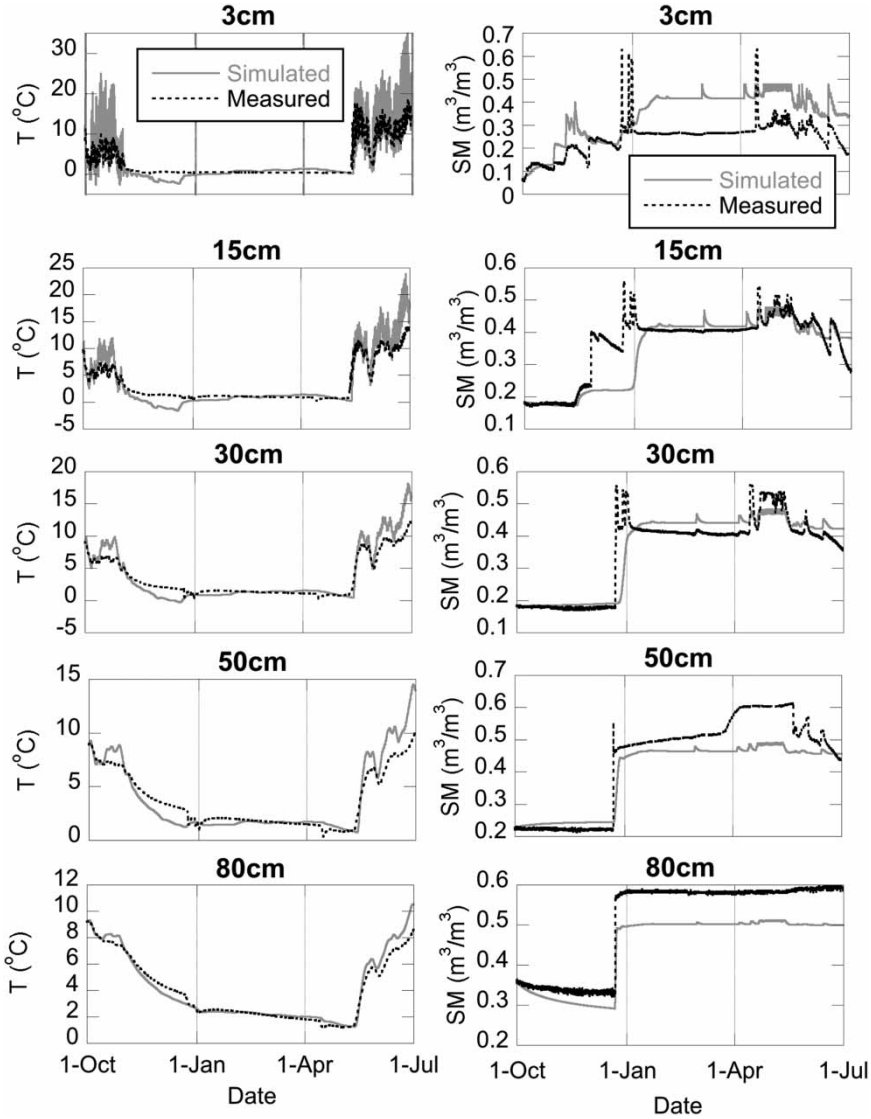

Figure 5 | Comparison between simulated and observed soil temperature (T) and soil moisture (SM) at different depths.

Table 2 | Root mean squared differences (RMSD) for soil temperatures at different depths, during snow-free periods, and the period where there is an established snow-pack (3rd November 2005–16th May 2006).

Depth (cm)	RMSD (°C) (snow-free)	RMSD (°C) (snow)
3	5.3	1.3
15	3.0	1.1
30	2.4	0.8
50	1.9	0.7
80	0.8	0.3

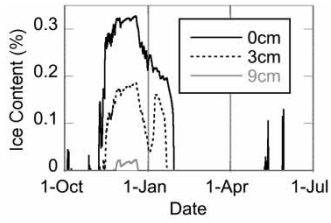

Figure 6 | Ice content simulated in surface and near-surface soil.

'standard' simulation, in which both the temperature and moisture conditions at the lower boundary vary in time in accordance with the observations. In this section, the effect of limited knowledge of the lower boundary conditions is examined, separately for the temperature and moisture conditions and also if both are poorly known.

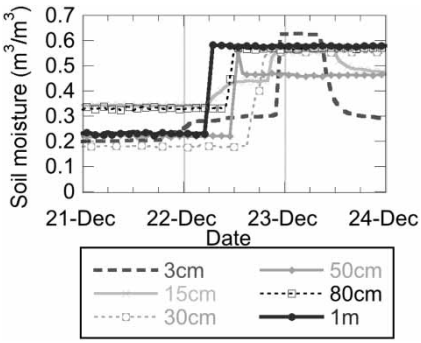

Figure 7 | Measured soil moisture changes at different depths over a 3-day period in December 2005.

Results from these simulations are compared to the standard simulation, and to the observations of temperature and moisture at different depths in the soil. For all these scenarios, the impact of the lower boundary condition on the SWE is small (RMSD changes from 49 mm to between 43 and 56 mm). Uncertainty in the lower boundary temperature had the greatest effect, but with no discernible change in shape in the SWE graph, these results have not been shown.

Figure 8 shows the impact of a poorly known lower boundary temperature, assuming that the soil moisture is well known. At the lower boundary, the minimum, the mean or the maximum soil temperatures were used for the simulations. Results were compared to the 'standard' simulation, where the temperature was fully specified, as well as to the measured values. At the surface, only the maximum temperature scenario had a significant effect, with the 3 cm soil temperature reaching a maximum of 5.6 °C. At greater depths, application of a maximum temperature lower boundary condition also had the greatest effect, although the 80 cm soil temperature simulated with the minimum temperature also deviated from the standard simulation and measurements in the first three months of the simulation. Uncertainty in the lower boundary condition had limited impact on the soil moisture at depths of 30 cm and greater. At the soil surface (3 cm), the maximum and minimum temperature lower boundary conditions affected the duration of frozen soil. In the maximum temperature case, the soil thawed earlier than in the standard simulation. For the minimum temperature scenario, thawing of the soil at a depth of 3 cm was prolonged and the soil moisture did not reach saturation until the end of April. This in turn influenced infiltration to the 15 cm layer, and simulated soil moisture at 15 cm is sensitive to the lower boundary temperature condition as a result of the freeze/thaw state of the layers above.

Figure 9 shows how well profiles of soil temperature and moisture may be simulated given good knowledge of the lower boundary temperature but poor knowledge of the soil moisture at the lower boundary. Soil temperatures are relatively unaffected by the soil lower boundary moisture. However, soil moisture at all depths is extremely sensitive to the lower boundary moisture condition. If maximum soil moisture is applied to the lower boundary, matric potential results in water flow up through the soil at the beginning of the season. This also happens to a lesser extent if the mean soil moisture is applied, although at a slower rate than for the maximum soil moisture case. At a depth of 3 cm, the differences are small between the standard simulation, the minimum and the mean soil moisture scenarios for the first 2.5 months of simulation. Use of minimum soil moisture as a lower boundary condition prevents saturation of the 3 cm soil surface layer, and the simulation gives good agreement with the observations for the period where a snowpack is established. However, the minimum moisture lower boundary condition has a dramatic effect on moisture deeper in the soil. Propagation of the wetting front up from the lower boundary is not simulated, and soil moisture at depths of 15 cm and greater only become saturated at the end of the snow ablation period, from infiltration of snow melt water.

Simulations of soil temperature and moisture profiles, given only mean values for the lower boundary conditions are presented in Figure 10. Soil temperature is relatively unaffected by the limited lower boundary conditions, with the simulated temperatures beginning to diverge from the measurements at a depth of 50 cm and deeper. Small differences in soil moisture occur between the completely specified ('standard') and mean-value simulations at 3 and 15 cm. At 30 cm, poor knowledge of the lower boundary conditions results in reasonable simulations after the wetting front has passed (in late December). Prior to this, the simulation indicates gradual wetting of the soil at 30 cm, which is in contrast to the dry nature of the soil at the start of the season. At 50 and 80 cm, the simulations are a poor indicator of the state of the soil.

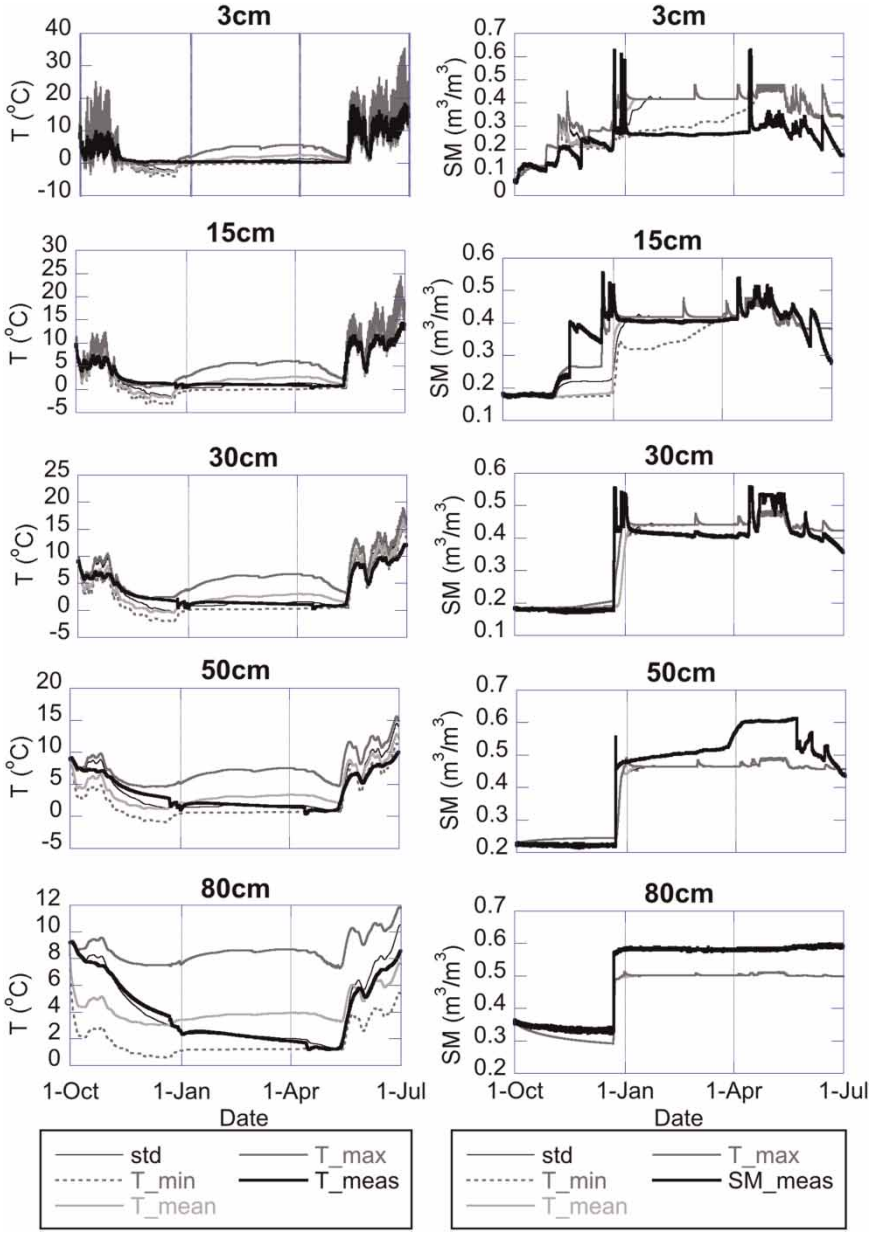

Figure 8 | Sensitivity of soil temperature (T) and moisture (SM) profiles to 1 m soil lower boundary temperature. T_meas and SM_meas are the observed values, and std is the standard simulation where the lower boundary conditions are known. In all cases the lower boundary soil moisture condition was derived from the time-varying observations.

DISCUSSION

This paper presents a physically-based model of the snow and soil that will be used to form the basis of a data assimilation system for retrievals of snow mass and soil moisture. The model was formed through coupling an existing snow energy and mass model (SNOBAL) with a multi-layer soil model (SHAW) that solves the mass and energy conservation equations for the soil. An evaluation of the simulated SWE shows that the uncoupled SNOBAL model is better statistically. For this simulation, however, the SWE from SNOBAL matched the observations closely for most of the season as a result of processes that occurred at the start of the season. In an early melt period, where the

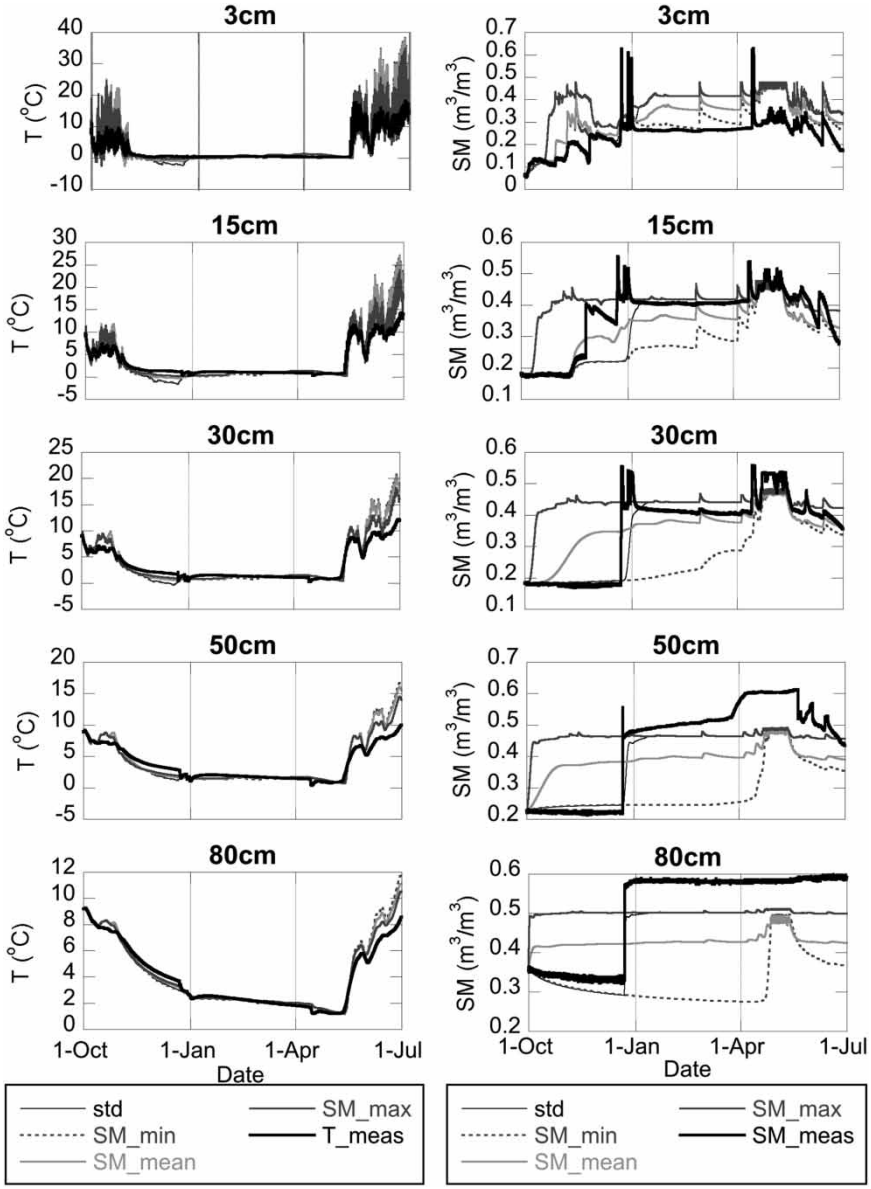

Figure 9 | Sensitivity of soil temperature (T) and moisture (SM) profiles to 1 m soil lower boundary soil moisture. T_meas and SM_meas are the observed values, and std is the standard simulation where the lower boundary conditions are known. In all cases, the temperature lower boundary condition was derived from the time-varying observations.

snowpack was also shallow, an overestimation of soil heat flux led to rapid melt in the simulation, and over half the thin snowpack was lost. Two subsequent melt periods occurred when the snow was thicker and was driven by the surface energy balance. For these periods, SNOBAL underestimated the rate of melt. The net effect of these processes is that the snow mass simulated by SNOBAL matched observations closely from this point and for the remainder of the season. SHAW coupled with SNOBAL simulated more realistic soil heat flux and rate of melt for the first melt period. Similar to the uncoupled SNOBAL, the rate of melt was also underestimated for two melt periods driven by surface energy exchanges. The net effect for the SNOBAL-SHAW simulation is a bias in the simulated SWE until the snow ablation period. This study highlights the importance of soil heat exchanges early in the season, whilst the snowpack is becoming established. As snow is deposited on the soil surface, the soil

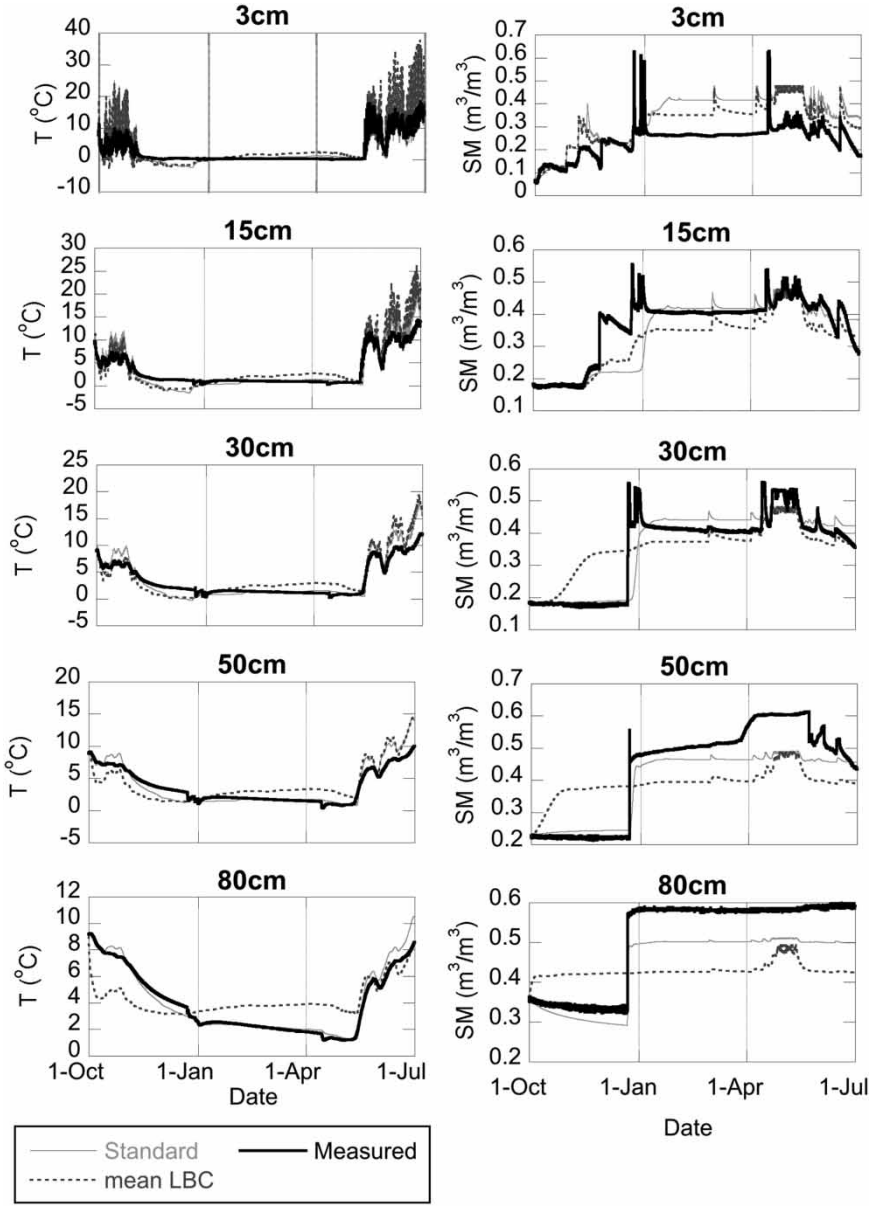

Figure 10 | Impact of mean values for soil temperature and moisture lower boundary conditions (mean LBC), compared to simulations where lower boundary values are specified from the measurements (Standard), and compared to observations (Measured).

temperature will determine whether the snow melts or is allowed to settle and decompose. The rate of change of the snow properties, e.g. crystal size, will also depend on the soil temperature. Thermal exchanges between snow and soil must be simulated accurately early in the season, as differences in snow mass and other snow properties at this point are carried through until the end of the season.

Coupling SHAW and SNOBAL is straightforward for the mass balance: snowpack outflow (melt and rain) is used as a source term at the soil surface. Linking the two models in the energy balance is more complicated. SHAW simulates the soil surface temperature (0 cm depth), but this should not be used to determine the soil heat flux. This surface temperature represents a very thin surface layer i.e. $\Delta z_g \rightarrow 0$, which makes the soil heat flux (Equation (5))

independent of the soil thermal conductivity and is not physically realistic. Also, the thermal inertia for a thin soil surface layer is small compared to the large snow base layer. Heat exchanges between these two layers would not affect the temperature of the snow layer significantly, but would change the temperature of the soil layer to approach that of the snow. By default, the thin soil surface layer freezes, which then impacts soil moisture. Addition of a thin layer at the base of the snow may allow soil surface temperature to be used to determine the soil heat flux, but is a significant increase in computational complexity. Global retrievals of snow mass requires modelling on a global scale, so a more efficient but less realistic approach was taken here, where the 30 cm soil temperature was used to link the energy balance of the snow and soil. This was chosen fairly arbitrarily as a balance between use of a near-surface temperature, and a large enough distance to avoid problems of surface freezing.

With this approach, profiles of soil temperature and moisture have been simulated with a reasonable degree of accuracy. The dynamic range of temperatures of the surface and near-surface soil is too high when snow is not present. This may impact the simulated SWE as temperatures that are too high or too low may hinder or enhance the accumulation of snow at the initialisation of the snowpack. In these simulations, freezing of the soil surface was simulated but not observed, and this affected soil moisture at the surface and infiltration into the layers below. Once the surface layers had thawed, liquid water was released for infiltration into lower layers. Thawing of the soil surface occurred after the lower layers had already saturated, so water flow was limited and the moisture content of the upper soil layer was higher than the observed values.

This is an unusual site, where soil moisture at depth can flip from extremely dry to extremely wet in the space of a couple of hours. The maximum observed value of soil moisture at the lower boundary was in excess of the saturation limit in the simulated soil. Although it is possible to adjust the soil parameters, we have chosen not to calibrate the model. Also, the density is a bulk property of the soil, so takes no account of local heterogeneity such as cracks, gaps and flow pathways that may contribute to additional moisture content around the sensor. Equation (11) was used to retrieve soil moisture from the observed dielectric constant. This relation is known to vary according to soil type, so use of this equation may have introduced a bias in the measured soil moisture.

The high rate of wetting at this site is partly due to its location in the basin, relatively low in elevation so receives meltwater from many parts of the basin. Rapid drainage channels are also suspected to form (Bathurst & Cooley 1996), which contribute to the high rate of change of soil moisture at the 1 m depth. To some extent, the model captures rapid wetting of the layers from the base through capillary uptake, although the wetting front in the simulations lags behind observations by increasing amounts higher in the soil profile. In the observations, rapid wetting of the soil at all depths occurs within a 24-hour period, so it is likely that lateral drainage is contributing to the large soil moisture change at all depths, and a 1-D model is not capable of simulating this process.

Application of the physically-based model beyond the point scale will mean that the lower boundary conditions will generally be known rather poorly, if at all. This study investigated the impact of the lower boundary conditions on the simulation of profiles of soil temperature and moisture. Limited knowledge of the soil temperature at a 1 m boundary affected temperatures deep in the soil, but only had a small effect at the soil surface. The lower boundary temperature condition did not affect soil moisture except in the case of frozen soil, where a change in the freeze/thaw state or proportion of ice in the soil matrix affected the soil water content and infiltration into lower soil layers. Soil temperatures are not affected by the soil moisture lower boundary condition. However, the soil moisture profile is extremely sensitive to the moisture at the lower boundary, as matric potential is governed by the availability of water at the boundary. The original hypothesis of this paper is that the lower boundary conditions do not affect the surface and near-surface soil temperature and moisture. Given the effect of even small changes in temperature on the freeze-thaw state of the soil, this hypothesis is rejected, whilst noting that the boundary conditions can be chosen carefully in order to produce reasonable simulations.

In terms of data assimilation, lack of knowledge of lower boundary conditions is not a problem for retrievals of snow mass, as the simulation of SWE is relatively insensitive to the soil temperature and moisture lower boundary.

However, this may be a problem for soil moisture data assimilation, where it is hoped that the surface soil moisture retrieved by satellite, e.g. by SMOS, can be related to moisture deeper in the soil to provide information on soil water availability for vegetation growth. An in-depth study is required to investigate how best to represent the soil if it is essentially unknown. SHAW allows the specification of different boundary conditions, such as application of a unit moisture gradient, which limits flow to gravitational only. This approach was used by Flerchinger *et al.* (1998) to evaluate simulations of surface fluxes and soil temperatures. Unfortunately soil moisture measurements were not available for evaluation as part of their study. SHAW can also allow the model to estimate the lower boundary temperature, as used by Preston & McBride (2004), who found that the mean difference between observed and simulated temperatures ranged between –0.1 and 1.6 °C for the upper 1 m of soil. Potentially, simulations could be improved with these alternative approaches.

Although the uncoupled SNOBAL model statistically showed better agreement with the measured SWE than the coupled SNOBAL-SHAW model for the data presented, it less suitable for the snow mass retrieval system (and cannot be used for retrievals of soil moisture). SNOBAL requires knowledge of near-surface soil temperatures, which will not be available on a global scale. The soil temperature will also govern the temperature gradient in the snow, which determines the rate of growth of snow grains. Snow grain size is a crucial parameter that determines the microwave behaviour of the snow, and must be known in order to make the snow mass retrievals.

Whilst it is desirable to have a close representation of physical reality as possible in a model, one of the benefits of data assimilation is that observations can be used to alter the model state. For example, retrievals of snow mass from satellite observations can be used to update snow mass in the model, therefore the bias in early season snow mass in the SNOBAL-SHAW coupled simulation should be removed as part of the assimilation process. Assimilation of the retrieved snow mass into the snow model can also be used to correct for processes not simulated by SNOBAL-SHAW. One example is blowing snow, which can change mass fluxes and incur additional sublimation losses. Use of the remote sensing observations to feed back the retrieved snow mass into the SNOBAL-SHAW model means that these processes do not need to be simulated explicitly.

Comparisons between the time-series of soil moisture observations and simulations should help diagnose model parameters and lower boundary conditions. As an example, if the simulated dry-down curve of the soil moisture is too shallow then this may identify deficiencies in the parameterisation or indicate too much moisture in lower layers. The interaction between surface wetness and surface water input may indicate the freeze-thaw state of the soil and whether this is represented adequately in the simulation. Fortunately the soil moisture satellite SMOS measures at L-band frequency (1.4 GHz), which means it is insensitive to the snow cover, provided the snow is not melting. SMOS has potential to be used directly to indicate whether the soil is frozen or unfrozen (e.g. Rautiainen *et al.* 2011), which in turn provides a temperature constraint in the model.

For retrievals of snow mass, independent estimates of snow properties from remote sensing observations will be used in the data assimilation system to constrain the parameters in the model. Techniques exist to retrieve surface snow grain size from optical sensors (Painter *et al.* 2009). Once the surface layer is buried by subsequent snowfalls, a physically-based model can be used to evolve the snow grains depending on the temperature of the snow and underlying soil. Scattering of microwave radiation is most sensitive to the grain size, so grain size needs to be known well in order to retrieve estimates of snow mass from passive microwave observations. Accurate simulation of the soil temperature is essential for good estimates of the snow grain size.

Quantitative analysis of model and observation error such as this is needed to determine the optimum method of blending the model and observations to get the best estimate of the state of the snow and soil. Once the data assimilation system have been developed, it can then be used to monitor changes in the snow and soil moisture. Dependent on the level of independent remote sensing data required to constrain the model, it may be possible to reprocess the historic dataset of passive microwave observations in order to determine whether snow mass has been changing over time in a similar manner to other parts of the Arctic.

ACKNOWLEDGEMENTS

Many thanks to Mark Murdock and Mark Seyfried for providing and advising on soil validation data. Thanks also to Michele Reba for providing and assisting with meteorological forcing data to drive SNOBAL. We also thank two anonymous reviewers whose thoughtful suggestions helped improve this paper.

REFERENCES

Barnett, T. P., Adam, J. C. & Lettenmaier, D. P. 2005 Potential impacts of a warming climate on water availability in snow-dominated regions. *Nature* **438**, 303–309.

Bathurst, J. C. & Cooley, K. R. 1996 Use of the SHE hydrological modelling system to investigate basin response to snowmelt at Reynolds Creek, Idaho. *J. Hydrol.* **175**, 181–211.

Brun, E., Martin, E., Simon, V., Gendre, C. & Coleou, C. 1989 An energy and mass model of snow cover suitable for operational avalanche forecasting. *J. Glaciol.* **35**, 333–342.

Chang, A. T. C., Foster, J. L. & Hall, D. K. 1987 Nimbus-7 SMMR derived global snow parameters. *Ann. Glaciol.* **9**, 39–44.

Davenport, I. J., Sandells, M. J. & Gurney, R. J. 2010 The effects of variation in snow properties on snow mass estimation using the Chang algorithm. In *Proc. British Hydrological Society Third International Symposium*, British Hydrological Society, Newcastle upon Tyne, pp. 846–850.

Dozier, J., Schneider, S. R. & McGinnis Jr., D. F. 1981 Effect of grain size and snowpack water equivalence on visible and near-infrared satellite observations of snow. *Water Resour. Res.* **17**, 1213–1221.

Flerchinger, G. N. 2000 *The Simultaneous Heat and Water (SHAW) Model: Technical Documentation*. Technical Report NWRC 2000-9s, June 15, 2000. Northwest Watershed Research Center, USDA Agricultural Research Service, Boise, Idaho.

Flerchinger, G. N. & Saxton, K. E. 1989 Simultaneous heat and water model of a freezing snow-residue-soil system I. Theory and development. *Trans. Am. Soc. Agric. Eng.* **32**, 565–571.

Flerchinger, G. N., Kustas, W. P. & Weltz, M. A. 1998 Simulating surface energy fluxes and radiometric surface temperatures for two arid vegetation communities using the SHAW model. *J. Appl. Meteorol.* **37**, 449–460.

Liang, X., Lettenmaier, D. P., Wood, E. F. & Burges, S. J. 1994 A simple hydrologically based model of land surface water and energy fluxes for general circulation models. *J. Geophys. Res.* **99**, D7, 14415–14428.

Male, D. H. 1980 The seasonal snowcover. In: *Dynamics of Snow and Ice Masses* (S. C. Colbeck, ed.). Academic Press, New York, pp. 305–395.

Marks, D. & Dozier, J. 1992 Climate and energy exchange at the snow surface in the Alpine region of the Sierra Nevada 2. Snow cover energy balance. *Water Resour. Res.* **28**, 3043–3054.

Marks, D., Kimball, J., Tingey, D. & Link, T. 1998 The sensitivity of snowmelt processes to climate conditions and forest cover during rain–on–snow: a case study of the 1996 Pacific Northwest flood. *Hydrol. Proc.* **12**, 1569–1587

Marks, D., Domingo, J., Susong, D., Link, T. & Garen, D. 1999 A spatially distributed energy balance snowmelt model for application in mountain basis. *Hydrol. Proc.* **13**, 1935–1959.

Marshall, S. E. & Warren, S. G 1987 Parameterization of snow albedo for climate models. In: *IAHS-AIHS Publication 166, 'Large Scale Effects of Seasonal Snow Cover'* (B. E. Goodison, R. G. Barry & J. Dozier, eds), IAHS, Wallingford, pp. 43–50.

Nayak, A., Marks, D., Chandler, D. G. & Seyfried, M. 2010 Long-term snow, climate and streamflow trends at the Reynolds Creek Experimental Watershed, Owyhee Mountains, Idaho, United States. *Water Resour. Res.* **46**, W06519.

Painter, T. H., Rittger, K., McKenzie, C., Slaughter, P., Davis, R. E. & Dozier, J. 2009 Retrieval of sub-pixel snow covered area, grain size and albedo from MODIS. *Remote Sens. Environ.* **113**, 868–879.

Preston, G. M. & McBride, R. A. 2004 Assessing the use of poplar tree systems as a landfill evapotranspiration barrier with the SHAW model. *Waste Manage. Res.* **22**, 291–305.

Rautiainen, K., Lemmetyinen, J., Pulliainen, J., Vehviläinen, J., Drusch, M., Kontu, A., Kainulainen, J. & Seppänen, J. 2011 L-Band radiometer observations of soil processes in boreal and subarctic environments. *IEEE Trans. Geosci. Remote Sens.* **99**, 1–15.

Seyfried, M. S., Grant, L. E., Du, E. & Humes, K. 2005 Dielectric loss and calibration of the Hydra Probe soil water sensor. *Vadose Zone J.* **4**, 1070–1079.

Winstral, A. & Marks, D. 2002 Simulating wind fields and snow redistribution using terrain-based parameters to model snow accumulation and melt over a semi-arid mountain catchment. *Hydrol. Process.* **16**, 3585–3603.

Zhang, T. 2005 Influence of the seasonal snow cover on the ground thermal regime: an overview. *Rev. Geophys.* **43**, RG4002.

First received 27 January 2011; accepted in revised form 26 September 2011. Available online 3 May 2012